Asymptotic instability of thin film flows subject to a step increase in Marangoni shear stress

By BENJAMIN J. FISCHER[1] AND SANDRA M. TROIAN[2]

[1]Aspen Technology, Inc., 200 Wheeler Road, Burlington, MA 01803

[2]California Institute of Technology, T. J. Watson Sr. Laboratories of Applied Physics, 1200 E. California Blvd, MC 128-95, Pasadena, CA 91125

Prior studies of a thin viscous film set in motion by a surface gradient in surfactant monolayer concentration have focused attention on the rapid film thinning near the initial edge of the coated film. Studies involving delivery of a *finite* and dilute mass of surfactant indicate transient amplification but eventual decay of spanwise disturbances localized at the raised edge of the advancing monolayer film. Studies involving continuous delivery according to $t^{1/2}$ have demonstrated more pronounced transient and asymptotic growth of upstream disturbances localized specifically within the thinning region. The onset times, however, exceed experimental observations by several orders of magnitude. In this work, a non-modal analysis describing sustained release by a source at the origin held at fixed concentration reveals prolonged amplification and asymptotic instability of disturbances within the thinning region for realistic onset times. More importantly, a reduced model which focuses on the step increase in shear stress just upstream of the minimum in film thickness reveals asymptotically unstable traveling waves in a reference frame situated within this inner region. The findings of this reduced model suggest more generally that lubrication flows subject to a step increase in shear stress, whether triggered by Marangoni, thermocapillary or other surface forces, are likely susceptible to a new type of interfacial instability.

1. Introduction

Control over the stress induced thinning and spreading rates of viscous films mobilized by gradients in surfactant surface concentration is key to a number of coating flows involving microscale liquid layers. The spatial and temporal behavior of the distorted film shape, flow speed and surface shear stress has been the subject of numerous theoretical studies because of the complex waveforms describing the base state profiles. The combined effect of Marangoni, capillary, viscous, gravitational and van der Waals forces is able to generate a wide spectrum of behavior whose response to perturbations in film thickness or concentration is still not completely understand. Experimental (Gaver & Grotberg 1992; Pereira 1995; Bull & Grotberg 2003; Dussaud, Matar & Troian 2005) and numerical studies (Borgas & Grotberg 1988; Troian, Herbolzheimer & Safran 1990; Espinosa 1991; Jensen & Grotberg 1992; Jensen 1994; Matar & Troian 1997, 1998) of thin films partially coated by soluble or insoluble surfactant have established an important and general feature of these flows; namely, the spontaneous flow of surfactant produces rapid film thinning near the initial edge of the coated film followed downstream by an

advancing rim where the monolayer ends and the shear stress vanishes. Experiments by a number of groups have also shown, however, that the region of most significant film thinning undergoes an instability resembling the formation of spanwise dendritic rivulets that severely compromise the uniformity of the spreading film (Troian, Wu & Safran 1989; Frank & Garoff 1995; Pereira 1995; He & Ketterson 1995; Fischer, Darhuber & Troian 2001; Cachile, Schneemilch, Hamraoui & Cazabat 2002).

Linear stability analyses based on non-normal mode decomposition by Matar & Troian (1998, 1999*a*) and Fischer & Troian (2003*a*) have shown that delivery of a *finite* dilute mass of insoluble surfactant can generate transient amplification of spanwise disturbances as they travel past the advancing rim. Once these disturbances move into the region of rapid film thinning, however, their amplitude is strongly damped and the perturbations decay. Inclusion of an attractive van der Waals term in the evolution equation for the film thickness helps sustain and even amplify perturbations within the thinned film region (Matar & Troian 1999*b*; Warner, Craster & Matar 2002*a*,*b*; Fischer 2003). Numerical studies of this behavior, however, indicate that such substantial perturbative growth is more closely related to cusp formation and film rupture i.e. Marangoni stresses enable rapid film thinning but are not primarily responsible for the van der Waals driven instability. The region characterized by rapid film thinning is clearly relevant in either case.

Numerical studies have shown that the rate of film thinning is strongly influenced by the choice of initial and boundary conditions describing surfactant distribution and delivery (Jensen & Grotberg 1992). Models of sustained surfactant release where the total mass disbursed scales in time as $t^{1/2}$ tend to generate more significant interfacial curvature and film thinning near the initial edge of the coated film (Fischer & Troian 2003*b*) in comparison to models assuming a finite mass of dilute surfactant (Fischer & Troian 2003*a*). A non-modal stability analysis has shown that sustained surfactant release can generate asymptotically unstable modes within the thinned region (even in the absence of van der Waals interactions) but onset times for instability can be a few orders of magnitude larger than experimental observations (Fischer & Troian 2003*b*). Based on these results, it seems that onset of a Marangoni driven fingering instability requires a sufficiently large surfactant source to trigger the necessary degree of film thinning.

This hypothesis is tested in this current work by implementing sustained release from a source whose surface concentration at the origin is fixed in time, which mimics an infinitely large surfactant reservoir. The film thickness and concentration (base-state) profiles in rectilinear geometry are developed in §2.1. The linearized disturbance equations for 2D perturbations are presented in §2.2. The non-uniform spatial and temporal behavior of the evolving base states causes the generalized disturbance operator to be non-normal and non-autonomous (Davis, Fischer & Troian 2003). As a first approximation, the non-autonomous operator is reduced to autonomous form in §3 by computing the eigenspectrum at fixed times t_c. These selected times correspond to the time scales at which the height and concentration (base-state) waveforms adopt quasi self-similarity. For sufficiently long times t_c, spanwise disturbances localize within the region of large shear stress which precipitates rapid film thinning, and a portion of the corresponding eigenspectrum lies in the positive half-plane. A stability analysis which retains the full time dependence is presented in §4, which reduces the system to an initial value problem based on perturbative growth *relative* of the evolving base states. This analysis confirms that spanwise disturbances localized to the region of rapid film thinning undergo sustained amplification and asymptotic instability. More importantly, the spreading dynamics reveals that Marangoni driven film thinning establishes a step increase in shear stress just upstream of the minimum in film thickness. A reduced model is presented in

§5 which describes the response of a flat thin film to a step change in shear stress. In a reference frame coincident with the inner region, the film exhibits a distinct traveling wave solution shown to be asymptotically unstable (stable) to spanwise disturbances situated near the step increase (decrease) in shear stress.

2. Governing Equations

The schematic diagram in figure 1 depicts the initial state of a thin viscous film of thickness h_c^*, viscosity μ^* and density ρ^*, partially coated by insoluble surfactant ($-L_c^* \leqslant x \leqslant L_c^*$) for a system in rectilinear geometry. The initial surfactant concentration is denoted by Γ_m^*; this distribution rapidly decays to zero at $\pm L_c^*$. The surfactant reduces the liquid surface tension from σ_o^* (uncontaminated value) to σ_m^* and the maximum spreading pressure responsible for film mobilization is given by $\Pi^* = \sigma_o^* - \sigma_m^*$. The system exhibits mirror symmetry about $x = 0$, where the x-coordinate denotes the streamwise direction, the y-coordinate denotes the direction normal to the solid substrate ($y = 0$) and the z-coordinate represents the spanwise (transverse) flow direction. In general, parameters marked by an asterisk reflect dimensional quantities.

The dimensionless values of the film thickness, $H(x, z, t)$, and surfactant concentration, $\Gamma(x, z, t)$, are scaled upon the initial film thickness, h_c^*, and the monolayer concentration, Γ_m^*. The liquid surface tension is normalized according to $\sigma = (\sigma^* - \sigma_m^*)/\Pi^*$. The streamwise ($x$) and transverse ($z$) coordinates are both scaled by L_c^* (and later rescaled in time changing to a moving reference frame coincident with the leading edge of the spreading film). The characteristic flow speed established by the Marangoni stress is given by $u_c^* = \varepsilon\Pi^*/\mu^*$ where the small parameter describing this lubrication flow is given by $\varepsilon \equiv h_c^*/L_c^*$. The streamwise u and transverse w components of the velocity field $\boldsymbol{V} = (u, v, w)$ are therefore scaled upon u_c^*. In according with the lubrication approximation, the component v normal to the substrate is instead normalized by εu_c^*. All time scales are normalized by the convective time representative of Marangoni dominated flow, $t_c^* = L_c^*/u_c^* = \mu^* L_c^*/\varepsilon\Pi^*$. The pressure distribution within the film is normalized by Π^*/h_c^*.

These scalings allow simplification of the continuity and Navier-Stokes equations according to the lubrication approximation, which assumes for flat geometries that $\varepsilon^2 \ll 1$ and $\varepsilon Re = \varepsilon\rho^* u_c^* h_c^*/\mu^* \ll 1$ where Re is the Reynolds number. The resulting governing equations for the velocity field are

$$0 = \frac{\partial u}{\partial x} + \frac{\partial v}{\partial y} + \frac{\partial w}{\partial z} \tag{2.1}$$

and

$$0 = -\frac{\partial p}{\partial x} + \frac{\partial^2 u}{\partial y^2} \ , \tag{2.2a}$$

$$0 = -\frac{\partial p}{\partial y} - Bo \ , \tag{2.2b}$$

$$0 = -\frac{\partial p}{\partial z} + \frac{\partial^2 w}{\partial y^2} \ , \tag{2.2c}$$

where $Bo = \rho^* g h_c^{*2}/\Pi^*$ is a modified Bond number based on the surfactant spreading pressure. At the liquid-solid interface $y = 0$, the no-slip and no-penetration conditions apply, for which

$$u = v = w = 0 \ . \tag{2.3}$$

The tangential and normal stress balances at the gas-liquid interface $y = H(x, z, t)$ are

$$\frac{\partial u}{\partial y} = \frac{\partial \sigma}{\partial x} \quad \text{and} \quad \frac{\partial w}{\partial y} = \frac{\partial \sigma}{\partial z} \tag{2.4}$$

and

$$p(x, y = H, z, t) = -\mathcal{C}\nabla^2 H \quad , \tag{2.5}$$

where the reference pressure outside the liquid film is chosen for convenience to equal zero. The dimensionless group $\mathcal{C} \equiv \varepsilon^2 \sigma_m^*/\Pi^*$ is related to the inverse of the usual capillary number $Ca = \mu^* u_c^*/\sigma_m^*$ according to $\mathcal{C} = \varepsilon^3/Ca$.

The evolution equation for the film thickness $H(x, z, t)$ is determined from the interfacial kinematic condition, which dictates that the gas-liquid interface is a material surface, i.e. $D(y-H)/Dt = 0$, where D/Dt denotes the material derivative. This relation reduces to $v = DH/Dt$ at $y = H(x, z, t)$ where v is the vertical component of the velocity field $\boldsymbol{V}$. Integrating the incompressible form of the continuity equation by parts and using this kinematic condition yields the governing equation for the dimensionless film height $H(x, z, t)$. The velocity field is substituted into a species mass balance to yield the governing equation for the dimensionless (insoluble) surfactant concentration $\Gamma(x, z, t)$. By applying a linear equation of state relating surface tension to the surfactant surface concentration, the evolution equations for the film thickness, $H(x, z, t)$, and surfactant concentration, $\Gamma(x, z, t)$, in the limit of negligible Bond number $Bo = \rho^* g h_c^{*2}/\Pi^*$, assume the form (Jensen & Grotberg 1992; Matar & Troian 1998; Fischer 2003)

$$\frac{\partial H}{\partial t} = \boldsymbol{\nabla} \cdot \left[\frac{1}{2} H^2 \boldsymbol{\nabla}\Gamma - \frac{\mathcal{C}}{3} H^3 \boldsymbol{\nabla}^3 H \right] \quad , \tag{2.6a}$$

$$\frac{\partial \Gamma}{\partial t} = \boldsymbol{\nabla} \cdot \left[\Gamma H \boldsymbol{\nabla}\Gamma - \frac{\mathcal{C}}{2} \Gamma H^2 \boldsymbol{\nabla}^3 H + \frac{1}{Pe_s} \boldsymbol{\nabla}\Gamma \right] \quad . \tag{2.6b}$$

Values of the surface Peclet number, $Pe_s \equiv (u_c^* L_c^*)/\mathcal{D}_s^* = (\Pi^* h_c^*)/\mu^* \mathcal{D}_s^*$ where $\mathcal{D}_s^*$ is the surfactant surface diffusion coefficient, exceeding approximately 10^4 provide negligible contribution to the concentration profiles.

2.1. *Base-state solutions*

To effect a change in reference frame coincident with the advancing front of the surfactant monolayer, Jensen & Grotberg (1992) introduced a self-similar coordinate, $\xi = x/t^a$, with variable transformations:

$$H_o(x, t) = h_o(\xi, t) \quad \text{and} \quad \Gamma_o(x, t) = \frac{g_o(\xi, t)}{t^b} \ . \tag{2.7}$$

These transformations reduce (2.6a) and (2.6b) to the forms

$$t\frac{\partial h_o}{\partial t} = a\xi h_{o\xi} + \frac{1}{2}\left(h_o^2 g_{o\xi}\right)_\xi - \frac{\mathcal{C}}{3t^{4a-1}} \left(h_o^3 h_{o\xi\xi\xi}\right)_\xi \quad , \tag{2.8a}$$

$$t\frac{\partial g_o}{\partial t} = a\xi g_{o\xi} + b g_o + \left(g_o h_o g_{o\xi}\right)_\xi - \frac{\mathcal{C}}{2t^{4a-1}} \left(g_o h_o^2 h_{o\xi\xi\xi}\right)_\xi + \frac{t^b}{Pe_s} g_{o\xi\xi} \quad . \tag{2.8b}$$

In this current work, the near ($x = 0$) and far field ($x = \infty$) boundary conditions applied to these equations are

$$h_{o\xi}(0, t) = 0 \ , \ h_{o\xi\xi\xi}(0, t) = 0 \ , \ \text{and} \ \ g_o(0, t) = t^b \ , \tag{2.9a}$$

$$h_o(\infty, t) = 1 \ , \ h_{o\xi}(\infty, t) = 0 \ , \ \text{and} \ \ g_o(\infty, t) = 0 \ . \tag{2.9b}$$

These boundary conditions reflect symmetry of the film thickness about the origin and a quiescent and surfactant-free liquid film in the far field. Most importantly, however, the third condition in (2.9*a*) allows for sustained release of surfactant at the origin.

As first shown by Jensen & Grotberg (1992), there exist self-similar solutions to (2.8*a*) and (2.8*b*) provided the capillary and diffusion terms can be neglected such that $\mathcal{C} = 1/Pe_s = 0$. Within this approximation, the constraint of self-similarity requires that $a = (1+\alpha)/3$ and $b = (1-2\alpha)/3$. The additional requirement that the total amount of surfactant disbursed remain bounded in time such that $M_{total}(t) = \int_0^\infty \Gamma_o(x,t)dx = Mt^\alpha < \infty$ where $\alpha > 0$ establishes that $b \geqslant 0$. Clearly, the case $\alpha = 1/2$, which yields $a = 1/2$ and $b = 0$, identifies the maximum possible rate of surfactant spreading for self-similar solutions.

The boundary conditions specified in (2.9*a*) and (2.9*b*), however, preclude the possibility of self-similarity even for the case $b = 0$, which corresponds to affixing the value of the surfactant concentration at the origin to unity. Furthermore, it is desirable to include the effects of capillarity and surface tension in order to describe more realistic systems. In this paper, the system of equations (2.8*a*) and (2.8*b*) is therefore solved as an initial value problem representing the configuration shown in figure 1. The initial conditions ($t = 1$) chosen for this study represent an initially flat liquid layer coated with an insoluble surfactant monolayer of extent $x \leqslant L_c^*$ whose concentration is relatively flat but smoothly decays to zero near the point $\xi = 0.5$:

$$h_o(\xi, t=1) = 1 \quad \text{and} \quad g_o(\xi, t=1) = \frac{1}{2}\ \{1 - \tanh\left[10(\xi - 0.5)\right]\} \quad . \tag{2.10}$$

All computations for this study were restricted to the parameter values $a = 0.45$ and $b = 0$ although the analytic derivations provided in the remainder of this paper allow for other choices as well. The choice $b = 0$ conveniently reduces the concentration boundary condition at the origin to unity i.e. $g_o(\xi = 0, t) = 1$, which in principle provides for an infinite source of surfactant to the spreading film. The value of the transformation constant a specifying the coordinate change $\xi = x/t^a$ was estimated by finding values which led to a good collapse of the numerical solutions for h_o and g_o at late times . The simple scaling argument shown next based on (2.6*a*) and (2.6*b*) indicates why a spreading monolayer driven solely by Marangoni stresses advances according to $x \sim (H_o\Gamma_o)^{1/2}t^{1/2}$, namely

$$\begin{aligned} \frac{\partial H_o}{\partial t} &\sim \frac{\partial}{\partial x}\left(H_o^2\Gamma_{ox}\right) \qquad \text{and} \qquad \frac{\partial \Gamma_o}{\partial t} \sim \frac{\partial}{\partial x}\left(H_o\Gamma_o\Gamma_{ox}\right)\ , \\ \frac{H_o}{t} &\sim \frac{H_o^2\Gamma_o}{x^2} \qquad \text{and} \qquad \frac{\Gamma_o}{t} \sim \frac{H_o\Gamma_o^2}{x^2}\ , \\ x &\sim (H_o\Gamma_o)^{1/2}\ t^{1/2} \quad \text{and} \quad x \sim (H_o\Gamma_o)^{1/2}\ t^{1/2} \quad . \end{aligned} \tag{2.11}$$

Capillary and surface diffusion effects reduce the value of a slightly below 1/2. In this work, the additional parameter values were held fixed at $Pe_s = 1000$ and $\mathcal{C} = 10^{-4}$.

Figure 2 shows the resulting spreading profiles for $h_o(\xi,t)$, $g_o(\xi,t)$ and $g_{o\xi}(\xi,t)$ for $1 \leqslant t \leqslant 10^4$, $Pe_s = 1000$ and $\mathcal{C} = 10^{-4}$. These solutions were obtained using the method of lines (see Schiesser 1991), which implements second-order centered differences for the spatial derivatives, and a fully implicit Gear's method for the time integration (see Hindmarsh 1983). The non-uniform mesh for integration consisted of 893 gridpoints over a domain length of 2.5. The density of points in the range $0 \leqslant \xi \leqslant 1$ was higher to obtain better resolution of the region undergoing rapid film thinning near $\xi \approx 0.6$ as well as the flat film near the origin. This mesh utilized grid-spacings of $\Delta\xi = 10^{-3}$ near $\xi = 0.6$ and $\Delta\xi = 3 \times 10^{-3}$ far downstream.

The non-uniform distribution of surfactant during film spreading generates significant film thinning centered near the initial monolayer decay point $\xi = 0.5$ followed downstream by an advancing rim whose position correlates with the end of the surfactant monolayer. The film depression deepens and widens with time. The boundary conditions for this system generate a concentration gradient $g_{o\xi}$ that is approximately constant for an extended region but decays sharply just behind the pinch point $\xi \approx 0.5$. The shear stress in the spreading film also peaks in value near the minimum in film thickness. The general shape of this shear stress profile and its implications for perturbative growth of spanwise disturbances constitutes the major focus of this work.

2.2. *Linearized disturbance equations*

Considered here are two dimensional disturbances to the spreading film with periodicity in the spanwise direction (z) characterized by wavenumber Q. The disturbance film thickness $\widetilde{H}(x,z,t)$ and surfactant concentration $\widetilde{G}(x,z,t)$ undergo a second transformation similar to that introduced in (2.7) to effect a change in reference frame coincident with the spreading front, namely

$$\widetilde{H}(x,\ z,\ t) = \Psi(\xi,\ t)\ e^{iQz} \quad \text{and} \quad \widetilde{G}(x,\ z,\ t) = \frac{\Phi(\xi,\ t)}{t^b}\ e^{iQz}\ . \tag{2.12}$$

Linearization of (2.6a) and (2.6b) according to these transformations yields the equation pair

$$\begin{aligned} t\frac{\partial \Psi}{\partial t} &= a\xi\Psi_\xi + \frac{1}{2}\big(h_o^2\Phi_\xi + 2h_o g_{o\xi}\Psi\big)_\xi - \frac{(Qt^a)^2}{2}h_o^2\Phi \\ &\quad - \frac{\mathcal{C}}{3t^{4a-1}}\ \Big[\big(h_o^3\Psi_{\xi\xi\xi} + 3h_o^2 h_{o\xi\xi\xi}\Psi\big)_\xi \\ &\quad - (Qt^a)^2\left(3h_o^2 h_{o\xi}\Psi_\xi + 2h_o^3\Psi_{\xi\xi}\right) + (Qt^a)^4 h_o^3\Psi\Big]\ , \qquad (2.13a) \\ t\frac{\partial \Phi}{\partial t} &= a\xi\Phi_\xi + b\Phi + \big(g_o g_{o\xi}\Psi + h_o g_{o\xi}\Phi + h_o g_o\Phi_\xi\big)_\xi - (Qt^a)^2 h_o g_o\Phi \\ &\quad - \frac{\mathcal{C}}{2t^{4a-1}}\ \Big\{\big(g_o h_o^2\Psi_{\xi\xi\xi} + 2g_o h_o h_{o\xi\xi\xi}\Psi + h_o^2 h_{o\xi\xi\xi}\Phi\big)_\xi \\ &\quad - (Qt^a)^2\left[(g_o h_o^2)_\xi\Psi_\xi + 2g_o h_o^2\Psi_{\xi\xi}\right] + (Qt^a)^4 g_o h_o^2\Psi\Big\} \\ &\quad + \frac{t^b}{Pe_s}\left[\Phi_{\xi\xi} - (Qt^a)^2\Phi\right]\ , \qquad (2.13b) \end{aligned}$$

This system of equations is conveniently expressed in matrix form:

$$t\ \frac{\partial \boldsymbol{u}}{\partial t} = \mathsf{A}(\xi, Q, t)\cdot\ \boldsymbol{u}\ , \tag{2.14}$$

where $\boldsymbol{u} = [\Psi,\ \Phi]$ represents a generalized disturbance vector and $\mathsf{A}(\xi,Q,t)$ denotes the linearized matrix operator. The time-dependence of the matrix A arises both from the explicit time dependent terms on the right hand side of (2.13a) and (2.13b) as well as the implicit time dependence inherent in the base-state variables $h_o(\xi,t)$ and $g_o(\xi,t)$.

The boundary conditions used for solution of (2.14) are:

$$\Psi_\xi(0,t) = 0\ ,\quad \Psi_{\xi\xi\xi}(0,t) = 0\ ,\quad \text{and}\quad \Phi_\xi(0,t) = 0\ , \tag{2.15a}$$

$$\Psi_\xi(\infty,t) = \Psi_{\xi\xi\xi}(\infty,t) = 0\quad \text{and}\quad \Phi(\infty,t) = 0\ . \tag{2.15b}$$

By allowing the slope but not the amplitude of $\Psi(\xi,t)$ to vanish in the far field $\xi \to \infty$, it is possible to recover bounded spatial oscillations far from the spreading front representative of capillary wave disturbances. This boundary condition therefore allows for simultaneous

solution of the continuous spectrum, as previously demonstrated for thin film spreading by gravity (Ye & Chang 1999) and thin film flow over topological features (Kalliadasis & Homsy 2001).

3. Eigenspectrum for Stationary Disturbance Operator

The non-uniform spatial and temporal behavior of the evolving base states causes the generalized disturbance operator $\mathsf{A}(\xi, Q, t)$ to be non-normal and non-autonomous (Davis, Fischer & Troian 2003). As a first approximation, the non-autonomous operator is reduced to stationary form $\mathsf{A}(\xi, Q, t_c)$ where the choice t_c corresponds to sufficiently late times when the base-state height and concentration profiles assume quasi self-similar form. The disturbances are assumed to evolve as a power law in time according to

$$\Psi(\xi, t) = \psi(\xi)\ t^{\beta} \quad \text{and} \quad \Phi(\xi, t) = \phi(\xi)\ t^{\beta} \ , \tag{3.1}$$

which reduces (2.14) to

$$\beta \widehat{\boldsymbol{u}} = \mathsf{A}(t_c)\ \cdot\ \widehat{\boldsymbol{u}} \ , \tag{3.2}$$

where $\widehat{\boldsymbol{u}} = [\psi,\ \phi]$ represents the generalized disturbance vector. The assumption of algebraic growth removes any explicit time-dependence on the left hand side of (2.14); this assumption, however, is equivalent to seeking solutions with exponential growth rates $\exp \beta\tau$ where $\tau = \ln t$. The eigenspectrum of $\mathsf{A}(t_c)$ therefore simply determines the disturbance growth rates $\beta(Q)$ within this stationary approximation.

As briefly discussed in §2.2, evaluation of the continuous spectrum identifies oscillatory disturbances in the far field not possible when decay boundary conditions are specified as $x \to \infty$. The eigenvalues corresponding to these modes can be obtained here by considering the limiting behavior of (2.13*a*) and (2.13*b*) as $\xi \to \infty$ subject to the far field constraints $h_o(\xi \to \infty, t) = 1$, $g_o(\xi \to \infty, t) = 0$, $\Psi_\xi(\xi \to \infty, t) = 0$ and $\Phi(\xi \to \infty, t) = 0$. Substitution of these boundary conditions reduces (2.13*a*) to

$$\beta\psi = -\frac{\mathcal{C}}{3t_c^{4a-1}} \left(\psi_{\xi\xi\xi\xi} - 2Q^2 t_c^{2a} \psi_{\xi\xi} + Q^4 t_c^{4a} \psi\right) \ . \tag{3.3}$$

Sinusoidal perturbations of the form $\psi \sim e^{is\xi}$ yield the dispersion relation $\beta(Q)$ governing the locus of the essential spectrum,

$$\beta = -\frac{1}{3}\mathcal{C} t_c^{1-4a} s^4 - \frac{2}{3}\mathcal{C} t_c^{1-2a} Q^2 s^2 - \frac{1}{3}\mathcal{C} t_c Q^4 \ . \tag{3.4}$$

Within the stationary approximation, this result confirms that all far field capillary wave disturbances decay as t^{β}. The maximum growth rate β defined by $s = 0$, specifies a wave of constant amplitude $\psi(\xi)$ and growth rate (in the moving frame of reference)

$$\beta = -\frac{1}{3}\mathcal{C} t_c Q^4 \ . \tag{3.5}$$

The eigenvalues and eigenvectors of (3.2), which correspond to the disturbance growth rate β and the (transformed) disturbance film thickness ψ and surfactant concentration ϕ, were calculated using the sparse eigenvalue solver EIGS in MATLAB. Figure 3 presents results for the instantaneous disturbance growth rate $\beta(Q, t_c)$ for $0 \leqslant Q \leqslant 15$. For times $t_c \lesssim 30$, the stationary base-states are stable to disturbances of all wavenumbers. For a large range in $t_c > 30$, the solutions for the $Q = 5$ and $Q = 10$ modes maintain a positive growth rate while disturbances with $Q = 15$ always decay. The $Q = 10$ mode achieves a maximum growth rate at $t_c \approx 250$ and re-enters the negative half-plane at $t_c \approx 650$. The eigenvalues and eigenvectors of $\mathsf{A}(t_c)$ could not be accurately obtained for $t_c > 10^3$

using the EIGS function in MATLAB 5.3. Numerical problems developed for evaluations at late times perhaps caused by the inherent non-normality of the disturbance operator. Since positive branches are evident at much earlier times, it was decided to investigate in more detail solutions based on the full time dependence of the underlying disturbance operator, as described in §4.

The growth rate and disturbance amplitudes, $\psi(\xi)$ and $\phi(\xi)$, for $t_c = 10$ are depicted in figure 4 for several choices of Q. The growth rates $\beta(Q, t_c = 10)$ shown in figure 4 (*a*) all lie in the negative half-plane for $Q \leqslant 15$. For small values of Q, the largest eigenvalue is dominated by the branch corresponding to the capillary-like disturbance specified in (3.5). This mode is designated by the abbreviation CW in figure 4 (*b*) and the associated concentration disturbance is shown in figure 4 (*c*). For wavenumbers $Q \gtrsim 4.9$, the largest eigenvalue corresponds instead to a branch of the discrete spectrum. Interestingly, the solutions corresponding to the discrete spectrum are highly localized to the region of rapid film thinning at $\xi = 0.6$ but their amplitude effectively vanishes everywhere else. By contrast, solutions of the continuous spectrum representing capillary-like disturbances peak in amplitude at the position of the leading edge $\xi = 1.8$ but also maintain smaller deflections near $\xi = 0.6$.

Representative base-states beyond $t = 30$ exhibit substantial film thinning near $\xi = 0.6$. If the stationary disturbance operator is evaluated at $t_c = 100$, solutions exhibit positive growth rates for $1 \leqslant Q \leqslant 13$ with a maximum value at $Q \approx 6$, as shown in figure 5 (*a*). For $t_c = 10$, the largest eigenvalue for small wavenumbers corresponds to the capillary-like disturbance, an example of which is shown in figures 5 (*b*) (as designated by the abbreviation CW) and 5 (*c*). By contrast with the results for $t_c = 10$, these solutions exhibit a maximum value at the minimum in (base-state) film thickness with smaller deflections centered about the leading edge. For $Q > 1$, the largest eigenvalue corresponds to solutions of the discrete spectrum, and the eigenfunctions, $\psi(\xi)$ and $\phi(\xi)$, peak in amplitude only in the vicinity of $\xi = 0.6$.

From these numerical studies, it is not surprising that the disturbance functions tend to localize to the region of rapid film thinning ($\xi = 0.6$) since here the concentration gradient $g_{o\xi}$ (or equivalently, the shear stress) exhibits a large spike, as evident in figure 2. This region is highly susceptible to perturbative growth (Fischer & Troian 2003*a*,*b*) provided the furrow is sufficiently deep. The stationary approximation shows, for example, that the growth rates corresponding to $t_c < 30$ for the parameter values examined, are strictly negative until the furrow has had sufficient time to thin and widen.

4. Linearized Transient Growth Analysis

A proper stability analysis of the linearized disturbance operator requires the full time dependence inherent in (2.14). Farrell & Ioannou (1996*b*) discuss that disturbance growth in non-autonomous systems can be monitored by the Lyapunov exponent. This method, however, is computationally prohibitive for these systems of equations since the time dependence of the evolving base states does not reduce to simple analytic form (Davis *et al.* 2003). As an alternative, the kinetic energy associated with the perturbations can be monitored with respect to the energy of the underlying base-states (Shen 1961). The ratio of the relative kinetic energy of the disturbance (d), $E_d(t)$, to that of the reference base state (b), $E_b(t)$, provides a convenient measure of disturbance growth at time t. Normalizing the energy of the base-states and disturbances by the corresponding values

at a reference time t_i leads to the amplification ratio

$$R = \left[\frac{E_d(t)}{E_d(t_i)}\right] / \left[\frac{E_b(t)}{E_b(t_i)}\right] \ , \tag{4.1}$$

which surveys the intensification or dissipation of the relative input energy over a given time interval. The normalized rate of disturbance growth is then given by $\Omega = R^{-1}dR/dt$. These measures combine the effects induced by the coupled field variables representing the film thickness and surfactant concentration in contrast with previous studies (Matar & Troian 1999*a*). The kinetic energies $E_b(t)$ and $E_d(t)$ averaged over a period $\lambda = 2\pi/Q$ are defined by

$$E_b \equiv \frac{1}{2\lambda}\int_0^{\lambda}\int_0^{\infty} |\langle \boldsymbol{V_o}\rangle|^2(\xi,t)\ d\xi\ dz \ , \tag{4.2a}$$

$$E_d \equiv \frac{1}{2\lambda}\int_0^{\lambda}\int_0^{\infty} |\langle \widetilde{\boldsymbol{V}}\rangle|^2(\xi,t)\ d\xi\ dz \ . \tag{4.2b}$$

The angular brackets denote the height averaged flow speed. The magnitude of the base-state velocity field is denoted by $|\langle \boldsymbol{V_o}\rangle|$, and that of the disturbance velocity field by $|\langle \widetilde{\boldsymbol{V}}\rangle|$. In particular, the height-averaged base-state streamwise and transverse flow fields, respectively, are given by

$$\langle u_o\rangle = -\frac{1}{2t^{a+b}}h_o g_{o\xi} + \frac{\mathcal{C}}{3t^{3a}}h_o^2 h_{o\xi\xi\xi} \ , \tag{4.3a}$$

$$\langle w_o\rangle = 0 \ , \tag{4.3b}$$

while the corresponding flow speed for the averaged disturbance fields are given by

$$\langle \widetilde{u}\rangle = \left[-\frac{1}{2t^{a+b}}\left(h_o\phi_\xi + g_{o\xi}\psi\right) + \frac{\mathcal{C}}{3t^{3a}}h_o\left(h_o\psi_{\xi\xi\xi} + 2h_{o\xi\xi\xi}\psi - t^{2a}Q^2h_o\psi_\xi\right)\right]e^{iQz} \tag{4.4a}$$

$$\langle \widetilde{w}\rangle = \left[-\frac{1}{2t^{a}}h_o\phi + \frac{\mathcal{C}}{3t^{2a}}h_o^2\left(\psi_{\xi\xi} - t^{2a}Q^2\psi\right)\right]iQe^{iQz} \ . \tag{4.4b}$$

By retaining the full time dependence of the base state solutions as well as the disturbance matrix, the stability analysis reduces to an initial value problem. The identification of "optimal disturbances", as has been demonstrated for certain coating flows which support time independent traveling wave base states (Davis & Troian 2003; Davis, Fischer & Troian 2003), is not possible for the system of equations shown here.

4.1. *Eigenvector disturbances*

For the parameter set of choice, the results of the stationary (modal) approximation in §3 indicate that film spreading supports positive disturbance growth rates for $t_c = 100$ but not $t_c = 10$. Further insight into film stability can be gained by evaluating the amplification ratio $R(t)$ resulting from specific initial film shapes and concentration profiles representing the eigenfunctions identified by the stationary approximation. In other words, the eigenfunction solutions with maximum growth rate β (examples of which are shown in figures 4 and 5) are deliberately applied to the spreading film and allowed to evolve according to (3.2), where $\mathsf{A} = \mathsf{A}(t_i)$ and where t_i is set equal either to $t_c = 10$ or $t_c = 100$. Figures 6*a* and *b* shows results of the computed amplification ratios $R(t)$ for $t_i = 10$ and $t_i = 100$, respectively, and $5 \leqslant Q \leqslant 25$. In figure 6 (*a*), the smallest wavenumber ($Q = 5$) undergoes the largest relative amplification. The initial amplification is small but by $t \approx 10^3$ attains a value exceeding 10^5. The $Q = 10$ and $Q = 15$ modes undergo an initial stabilizing response manifested by a decrease in $R(t)$ but these too undergo

substantial amplification for $t > 100$. By contrast, the smallest wavelength disturbance, $Q = 25$, suffers progressive decay. If instead the selected perturbations corresponding to $t_i = t_c = 100$ are applied to the spreading film, the modes $Q = 5$ and 10 amplify immediately. After a brief stabilizing period, the $Q = 15$ mode also attains an amplification ratio of about 200 by $t = 10^4$. Similar to figure 6 (*a*), the smallest wavelength disturbance, $Q = 25$, again suffers progressive decay.

Such large amplification ratios coincide with large increases in the amplitudes of the disturbance functions $\Psi(\xi, t)$ and $\Phi(\xi, t)$. For example, figure 7 shows the evolution of perturbations applied at $t_i = 100$ for $Q = 5$. These disturbances strongly localize to the region of high shear stress (spike in $g_{o\xi}$) because of the rapid film thinning demonstrated by the base state. The superposition $h(\xi, z, t) = h_o(\xi, t) + \tilde{\delta}\Psi(\xi, t)\sin(Qz)$ is shown in figure 8 for $Q = 5$, $t = 500$, and $\tilde{\delta} = 0.01$. In this example, the spanwise disturbances generate corrugations in the spreading layer just behind the thinnest portion of the film.

4.2. *Localized Perturbations*

Gaussian perturbations of the form

$$\Psi(\xi, t = 1) = \Phi(\xi, t = 1) = \ e^{-50\ (\xi - \xi_s)^2}\ . \tag{4.5}$$

were also examined in order to determine what is the influence of the position ξ_s on disturbance amplification. Without loss in generality, the amplitudes $\Psi(\xi, t = 1)$ and $\Phi(\xi, t = 1)$ are set to unity since equations (2.13*a*) and (2.13*b*) are linear. In a previous study (Fischer & Troian 2003*a*; Fischer 2003), it was shown that disturbances convecting past the advancing rim of the film experience a transient boost in amplitude (in the moving reference frame) but rapid decay once these reach the furrow upstream. It was also noted that disturbances initially situated further from the advancing front undergo larger amplification since the waveform corresponding to the base state has additional time to develop a thicker rim. The results of the amplification studies in figure 9 for $0 \leqslant Q \leqslant 15$ and initial placements $\xi_s = 1.0$ and 2.0 confirm a similar view. The onset time for the initial boost in amplitude is delayed with increasing ξ_s since the disturbance must travel upstream (in the moving reference frame) a longer distance before contacting the rim. More importantly, however, these results show that amplification resumes as the disturbances localize within the furrow upstream although the amplification ratio for these types of Gaussian perturbations is overall still small.

5. Model Reduction and Physical Mechanism Responsible for Unstable Spreading

The physical understanding resulting from the data in §3 and §4 can be summarized as follows. For sustained growth of disturbances and asymptotic instability, there needs to develop a sufficiently deep and wide furrow in the upstream region, as indicated in figure 2 (*a*). This process leas to a steep decay in the value of $g_{o\xi}$, or equivalently a steep increase in the value of the shear stress $-g_{o\xi}$, just upstream of the minimum in film thickness, as shown in figure 2 (*c*). It is this important feature that is approximated below within the reduced model - namely, the response of an initially flat film to a step jump in shear stress in a reference frame moving with the "inner" rapidly thinned region.

The surface flow speed also exhibits a step increase near the furrow as evident in figure 10 for $t = 10^4$. The non-zero flow speed at $\xi = 0$ indicates the pull of liquid away from the origin. This non-vanishing shear stress is caused by the continuous supply of surfactant at the origin where the concentration is held fixed. This behavior is not observed in

model studies of the spread of a small and finite mass of surfactant, where the shear stress at the origin vanishes identically (Fischer & Troian 2003*a*). As with the behavior of the evolving shear stress, the surface speed increases slowly with ξ for $0 \leqslant \xi \lesssim 0.5$ but undergoes a significant step increase near the pinch point [see figure 2 (*a*)].

As discussed in §4, the linearized disturbance operator which retains the complete time dependence is non-autonomous and non-normal. However, it is possible to develop an autonomous disturbance matrix by appealing to a reduced model which focuses exclusively on the dynamics in the inner region of the flow situated just upstream of the furrow, as indicated in figure 11. Familiarity with a simpler class of lubrication flows describing film spreading by constant thermocapillary (Troian *et al.* 1990; Davis & Troian 2003; Davis *et al.* 2003), gravitational (Huppert 1982; Bertozzi & Brenner 1997), or centrifugal forces (Melo, Joanny & Fauve 1989; Fraysse & Homsy 1994) suggests advantages to be gained by mapping the inner region of the surfactant problem to alternative flows also described by non-normal operators.

The fingering patterns observed in these other coating flows, however, in no way resemble the arterial fingering patterns commonly observed in surfactant driven spreading where there occurs finger branching and tip-splitting (Fischer, Darhuber & Troian 2001). Instead the pressure distribution behind the moving contact line of a liquid film driven to spread across a dry substrate causes a recirculating flow and distinct bulge at the leading edge. This bulge, sometimes called a capillary rim, originates with the balance between the driving force for spreading, capillary and viscous forces. This balance establishes a characteristic length scale $\ell = h_{outer}/Ca^{1/3}$ (Troian, Herbolzheimer & Safran 1990; Kataoka & Troian 1997) where h_{outer} denotes the film thickness in the (upstream) outer region. The fingering instability in such systems resembles a lateral breakup of the capillary rim which generates an advancing parallel array of flowing rivulets, as observed in wet paint streaming down a vertical wall. The wavelength corresponding to the rivulet spacing is proportional to the dynamic capillary length ℓ. As discussed previously (Fischer & Troian 2003*a*; Fischer 2003), however, the dendritic instability observed in surfactant coated films develops specifically in the rapidly thinned region and not at the leading edge of the film. Nonetheless, the model reduction described below helps isolate the physical mechanism responsible for unstable flow in Marangoni driven spreading. Conceptually, then, the inner region sketched in figure 11 corresponds to the region of the film shown in figure 2 where the shear stress undergoes a step increase just upstream of the pinch point.

5.1. *Governing equations*

It proves useful for this part of the study to return to the dimensional form of the evolution equations for the film thickness $H^*(x, z, t^*)$ and surfactant equation $\Gamma^*(x, z, t^*)$ describing Marangoni driven spreading, namely

$$\frac{\partial H^*}{\partial t^*} + \boldsymbol{\nabla} \cdot \left[\frac{H^{*2}}{2\mu^*} \boldsymbol{\nabla} \sigma^* + \frac{\sigma}{3\mu^*} H^{*3} \boldsymbol{\nabla}^3 H^* \right] = 0 \quad , \tag{5.1a}$$

$$\frac{\partial \Gamma^*}{\partial t^*} + \boldsymbol{\nabla} \cdot \left[\frac{H^* \Gamma^*}{\mu^*} \boldsymbol{\nabla} \sigma^* + \frac{\sigma}{2\mu^*} \Gamma^* H^{*2} \boldsymbol{\nabla}^3 H^* \right] = 0 \quad , \tag{5.1b}$$

where surface diffusion is neglected and the surface tension associated with capillary effects is replaced by the value of the monolayer coated film σ_m^*.

To determine the proper scaling relationships within the inner region, all streamwise and transverse coordinate values are scaled by the characteristic length ℓ_c^* (whose value is determined below) and the film thickness by the initial film thickness h_c^*. The driving

stress $\boldsymbol{\nabla}\sigma^*$ is scaled upon a maximum value G_c^* representative of this region and the characteristic flow speed and convective time scales are given by $u_c^* = h_c^* G_c^*/(2\mu^*)$ and $t_c^* = \ell_c^*/u_c^*$, respectively. The extent of the inner region can then be determined by the balance in equation (5.1a) between the Marangoni and capillary fluxes such that $\ell_c^* = \sqrt[3]{2\sigma_m^* {h_c^*}^2/(3G_c^*)} = h_c^* \, (3Ca)^{-1/3}$ where $Ca = \mu^* u_c^*/\sigma_m^*$. These scaling relations for the inner region therefore reduce (5.1a) and (5.1b) to the form

$$\frac{\partial H}{\partial t} + \boldsymbol{\nabla} \cdot \left[H^2 \boldsymbol{\nabla}\sigma + H^3 \boldsymbol{\nabla}^3 H \right] = 0 \quad , \tag{5.2a}$$

$$\frac{\partial \Gamma}{\partial t} + \boldsymbol{\nabla} \cdot \left[2H\Gamma \boldsymbol{\nabla}\sigma + \frac{3}{2}\Gamma H^2 \boldsymbol{\nabla}^3 H \right] = 0 \quad . \tag{5.2b}$$

The parameter values $\Gamma = 0$ and $\boldsymbol{\nabla}\sigma$ equal to a constant describe film spreading by a constant thermocapillary force, as examined in detail elsewhere (Kataoka & Troian 1997, 1998; Davis, Fischer & Troian 2003).

5.2. *Base-state solutions for prescribed shear stress distributions*

The most important aspect of this model reduction consists of decoupling (5.2a) and (5.2b) by solving (5.2a) subject to a prescribed shear stress profile of the form

$$\sigma_x \to 1 \qquad \text{as} \quad x \to -\infty \qquad \text{(upstream)} \qquad \text{and} \tag{5.3a}$$

$$\sigma_x \to G \qquad \text{as} \quad x \to +\infty \qquad \text{(downstream)} \; , \tag{5.3b}$$

where the constant $G \geqslant 0$. This allows identification of traveling wave solutions for the base state film thickness in a reference frame moving at a constant speed c situated in the inner region. The transformation is given by $\xi = x - ct$. In this study, the step change in shear stress was modeled according to

$$\sigma_\xi = 1 + (G-1)\left[0.5 + \frac{1}{\pi} \arctan\left(\frac{\xi}{\delta} \right) \right] \quad . \tag{5.4}$$

This distribution includes three interesting cases depending on the range of values for G. Choices such that $G > 1$ mimic a step jump in shear stress as observed in the surfactant spreading problem. The choice $G = 1$, for which the shear stress is a constant over the entire (inner) spatial domain, describes the case of thermocapillary spreading (Kataoka & Troian 1997, 1998; Davis, Fischer & Troian 2003). Finally, choices corresponding to $G < 1$ describing a step-drop in shear stress, are useful in describing the behavior at the leading edge of the spreading monolayer [see figure 2 (c)] demonstrated within the complete model to be asymptotically stable (Fischer 2003).

The evolution equation describing the film thickness in rectilinear geometry is then given by

$$c h_{o\xi} - \left(\sigma_\xi h_o^2 + h_o^3 h_{o\xi\xi\xi} \right)_\xi = 0 \quad , \tag{5.5}$$

(where the subscript ξ indicates differentiation) subject to the boundary conditions

$$h_o \to 1 \quad \text{and} \quad h_{o\xi\xi\xi} \to 0 \qquad \text{as} \quad \xi \to -\infty \qquad \text{(upstream)} \tag{5.6a}$$

$$h_o \to h_\infty \quad \text{and} \quad h_{o\xi\xi\xi} \to 0 \qquad \text{as} \quad \xi \to +\infty \qquad \text{(downstream)} \; . \tag{5.6b}$$

Integration of (5.5) subject to (5.6a) and (5.6b), as well as the far field limits given by (5.3a) and (5.3a), establish a third-order ordinary differential equation for the base state film thickness

$$h_{o\xi\xi\xi} = \frac{c(h_o - 1) - \sigma_\xi h_o^2 + 1}{h_o^3} \quad , \tag{5.7}$$

where the characteristic speed of the inner region is given by

$$c = \frac{1 - Gh_\infty^2}{1 - h_\infty} \quad . \tag{5.8}$$

Solution of (5.7) proceeds by conversion to three first-order equations subsequently solved as initial value problems. This method of solution is commonly used for solution of free-surface lubrication flows. The starting value for integration at $\xi \to -\infty$ is obtained by linearizing (5.7) about the asymptotic value $h_o \to 1$. The first-order term in this expansion in given by

$$h_1 = c_1 \exp\left[(c-2)^{1/3}\xi\right] + c_2 \exp\left[-\frac{1}{2}(c-2)^{1/3}(1+i\sqrt{3})\xi\right] + c_3 \exp\left[\frac{1}{2}(c-2)^{1/3}(-1+i\sqrt{3})\xi\right] \quad , \tag{5.9}$$

In order for this expansion to remain bounded in the limit $\xi \to -\infty$, the asymptotic film thickness required for forward integration must satisfy the following constraints based on the wave speed c:

$$h_o = 1 + \tilde{\epsilon} \exp\left[(c-2)^{1/3}\xi\right] \quad \text{for} \quad c > 2 \tag{5.10a}$$

$$h_o = 1 + \tilde{\epsilon} \exp\left[-\frac{1}{2}(c-2)^{1/3}\xi\right] \cos\left[\frac{\sqrt{3}}{2}(c-2)^{1/3}\xi\right] \quad \text{for} \quad c < 2 \tag{5.10b}$$

$$h_o = 1 + \tilde{\epsilon} \quad \text{for} \quad c = 2 \quad , \tag{5.10c}$$

where $\tilde{\epsilon} \ll 1$ is the linearization parameter (not to be confused with the lubrication parameter ϵ. The complete solution for h_o is then found by forward integration ($\xi \to +\infty$) and the parameter $\tilde{\epsilon}$ is adjusted until the boundary conditions in (5.6*b*) are satisfied.

Figure 12 (*a*) shows examples of prescribed distributions in surface shear stress for three values of G and $\delta = 0.1$. Figure 12 (*b*) shows the corresponding traveling wave solutions for $h_\infty = 1/6$. (These steady states solutions require that the liquid flux be constant throughout the domain; as such, only certain values of h_∞ satisfy this requirement.) For each wave shown, the wave speed $c < 2$. These solutions are characterized by a distinct bulge just behind the location of the step change in shear stress where the maximum height increases with decreasing values of G. Smaller values of G generate higher wave speeds c which causes the liquid flux and therefore the bulge height to increase also.

For $G = 1$ (as in thermocapillary flow), the wave speed reduces to the value $c = 1 + h_\infty$, which increases linearly with the asymptotic value h_∞. For $h_\infty < 1$, the wave speed $c < 2$ and a characteristic bulge forms. For $G = 2$, the wave speed is a parabolic function of h_∞ and two distinct values of the asymptotic film thickness h_∞ can generate the same positive wave speed for $h_\infty < 2^{-1/2}$. The second solution for $G = 2$ and $h_\infty = 1/6$ is shown in figure 13. In contrast to the solution shown in figure 12 (*b*), here the upstream portion of the film exhibits some weak oscillations. The choice $G = 0.5$ generates a wave speed that monotonically increases h_∞. Provided $h_\infty < 2/3$, the wave speed is less than 2 which leads a bulge in the traveling wave.

5.3. *Disturbance equation for prescribed shear stress distribution*

Based on this reduced model, the evolution equation describing the disturbed film thickness $\widetilde{H}(x, z, t) = \Psi(\xi, t)e^{iQz}$, where the spanwise wavenumber Q is scaled upon the inner

length scale ℓ_c^*, is given by

$$\frac{\partial \Psi}{\partial t} = \frac{\partial}{\partial \xi}\left[c\Psi - 2\sigma_\xi h_o \Psi - h_o^3 \Psi_{\xi\xi\xi} - 3h_o^2 h_{o\xi\xi\xi}\Psi + Q^2 h_o^3 \Psi_\xi\right] + Q^2 h_o^3 \Psi_{\xi\xi} - Q^4 h_o^3 \Psi \quad (5.11)$$

subject to the boundary conditions

$$\Psi_\xi = \Psi_{\xi\xi\xi} = 0 \quad \text{as} \quad \xi \to \pm\infty \quad . \quad (5.12)$$

The stress profile σ_ξ is given by (5.4).

The equation describing the asymptotic behavior of $\Psi(\xi, t)$ as $\xi \to -\infty$ can be obtained by applying the boundary conditions in (5.6*a*):

$$\frac{\partial \Psi}{\partial t} = -\Psi_{\xi\xi\xi\xi} + 2Q^2 \Psi_{\xi\xi} - Q^4 \Psi \quad . \quad (5.13)$$

The substitution $\Psi(\xi, t) \sim e^{\beta t + is\xi}$ yields an expression for the disturbance growth rate

$$\beta(Q) = -s^4 - 2Q^2 s^2 - Q^4 \quad . \quad (5.14)$$

Spatially uniform disturbances in the upstream far field such that $s = 0$ exhibit negative growth rates

$$\beta = -Q^4 \quad . \quad (5.15)$$

In the opposite limit as $\xi \to +\infty$, the evolution equation derived from the boundary conditions in (5.6*b*) is given by

$$\frac{\partial \Psi}{\partial t} = -h_\infty^3 \Psi_{\xi\xi\xi\xi} + 2Q^2 h_\infty^3 \Psi_{\xi\xi} - Q^4 h_\infty^3 \Psi \quad , \quad (5.16)$$

which for disturbances of the form $\Psi(\xi, t) \sim e^{\beta t + is\xi}$, yields the expression for the growth rate

$$\beta = -h_\infty^3 s^4 - 2Q^2 h_\infty^3 s^2 - h_\infty^3 Q^4 \quad . \quad (5.17)$$

Spatially uniform disturbances in the downstream far field such that $s = 0$ also exhibit negative growth rates according to

$$\beta = -h_\infty^3 Q^4 \quad . \quad (5.18)$$

For $h_\infty \leqslant 1$, the values (5.18) are less negative than (5.15) and will therefore dominate the continuous eigenspectrum.

5.4. *Modal disturbance analysis*

General perturbations of the separated form $\Psi(\xi, t) = \psi(\xi)\ e^{\beta t}$ lead to a disturbance function for the film thickness described by the matrix equation

$$\beta \boldsymbol{u} = \mathsf{A} \cdot \boldsymbol{u} \quad , \quad (5.19)$$

where $\boldsymbol{u}$ is a vector consisting of the values of the disturbance ψ at discrete points of the spatial domain $(-\infty, +\infty)$. The disturbance operator A is autonomous in the moving frame of reference defined by $\xi = x - ct$ but non-normal due to the spatial inhomogeneity of the traveling base-state solution (Davis, Fischer & Troian 2003). In §5.5 is presented a linear stability analysis appropriate for non-normal operators. In this section, the eigenvalues and eigenfunctions corresponding to (5.19) are evaluated and discussed. Solutions to (5.19) were computed using the sparse matrix eigenvalue solver EIGS in MATLAB 5.3.

The results in figure 14 (*a*) show the computed growth rates $\beta(Q)$ corresponding to the base-states $h_o(\xi)$ in figure 12. In all three cases shown, there is a band of wavenumbers

for which the base states are asymptotically unstable in the moving reference frame. As G increases, the range in Q for instability as well as the maximum growth rate increase despite the fact that the bulge height in the base state profile decreases with increasing G. The results for $G = 1$ correspond exactly to previous solutions investigated by Troian *et al.* (1990) and Kataoka & Troian (1997, 1998) for $0.01 \leqslant h_\infty \leqslant 0.9$ where $\beta > 0$ for $0 < Q \lesssim 0.55$ with a most unstable wavelength $Q_{\max} \approx 0.35$. The values in table 1 clearly show that as the value of the shear stress ahead of the furrow increases from 0.5 to 2.0, so too does the maximum growth rate $\beta_{\max}$ and the corresponding wavenumber $Q_{\max}$ for $h_\infty = 1/6$. Furthermore, the eigenspectrum is dominated by the discrete spectrum for which the leading eigenfunctions $\psi(\xi)$ decay as $\xi \to \pm\infty$, as shown in figure 14 (*b*). These solutions have been normalized such that $(\int_0^\infty \psi^2 d\xi)^{1/2} = 1$. All three solutions exhibit a strong peak localized to the bulge region of the corresponding base-states. The peak magnitudes in ψ increase with increasing values of the shear stress G.

It has been previously noted (Troian, Herbolzheimer & Safran 1990) that the eigenfunction corresponding to the neutrally stable solution $\psi[\beta(Q = 0) = 0]$ is linearly proportional to $h_{o\xi}$ for films driven to spread by *spatially uniform* body or shear forces. This is a consequence of the translational invariance of the disturbance operator $\mathcal{L}_0$ which is independent of ξ. In this study, the prescribed jump in shear stress described by (5.4) for $G \neq 1$ imposes a spatially non-uniform stress. As shown next, the neutrally stable eigenfunction therefore violates this condition of proportionality. In the limit $\beta(Q = 0) = 0$, (5.11) reduces to

$$\begin{aligned} 0 &= \frac{\partial}{\partial\xi}\left[c\psi - 2\sigma_\xi h_o\psi - h_o^3\psi_{\xi\xi\xi} - 3h_o^2 h_{o\xi\xi\xi}\psi\right] \\ &= \left[\left(-2\sigma_\xi h_{o\xi} - 2\sigma_{\xi\xi}h_o\right) + \left(c - 2\sigma_\xi h_o\right)\frac{\partial}{\partial\xi} - 3h_o^2 h_{o\xi}\frac{\partial^3}{\partial\xi^3} - h_o^3\frac{\partial^4}{\partial\xi^4}\right]\psi \ , \qquad (5.20) \\ &= \mathcal{L}_0\psi \ . \qquad (5.21) \end{aligned}$$

where $\mathcal{L}_0$ is the linearized disturbance operator. Substitution of the relations $\psi(\xi) \propto h_{o\xi}$ and (5.7) into (5.21) yields

$$0 = -2\sigma_\xi h_{o\xi}^2 - 4\sigma_{\xi\xi}h_o h_{o\xi} - \sigma_{\xi\xi\xi}h_o^2 + \left(c - 2\sigma_\xi h_o\right)h_{o\xi\xi} - 3h_o^2 h_{o\xi}h_{o\xi\xi\xi} - h_o^3 h_{o\xi\xi\xi\xi} \ . \qquad (5.22)$$

When σ_ξ is a constant throughout the spatial domain (as for the case $G = 1$), $\sigma_{\xi\xi} = \sigma_{\xi\xi\xi} = 0$, and (5.22) reduces to

$$0 = ch_o h_{o\xi\xi} - 3h_o^2 h_{o\xi}h_{o\xi\xi\xi} - h_o^3 h_{o\xi\xi\xi\xi\xi} = \mathcal{L}_0 h_{o\xi} \ . \qquad (5.23)$$

confirming $\psi(\xi) \propto h_{o\xi}$ for $Q = 0$. For choices $G = 0.5$ or 2.0 in (5.4), the neutrally stable modes differ substantially from $h_{o\xi}$, as shown in figure 15.

5.5. *Non-modal disturbance analysis*

The linearized operator described by (5.19) is non-normal. It is known that nonorthogonality of modes in a non-normal system may lead to transient growth and disturbance amplification far in excess of that anticipated from the decay rates given by the eigenvalues of the operator (Farrell & Ioannou 1996*a*). The growth rates predicted from a normal mode analysis of the non-normal operator coincide with its eigenvalues only in the limit $t \to \infty$. At short or intermediate times, the maximum disturbance amplification is instead described by $\ln \|\exp(\mathsf{A}t)\|$, where $\|\cdot\|$ is evaluated in the L_2 norm. A more complete description of the fundamentals underlying a transient growth analysis of non-normal operators pertinent to free surface lubrication flows, as well as discussion of optimal disturbances, can be found in Davis *et al.* (2003). For this study, the amplification ratios were computed using the EXPM function in MATLAB 5.3.

Figure 16 shows the evolution of $\ln \| \exp(\mathsf{A}t) \|$ for optimal disturbances applied to the base states shown in figure 12. These disturbances generate the maximum possible amplification at time t. For the parameter values shown, the amplification shows a brief period of non-normal growth which rapidly transitions to the value $\ln \| \exp(\lambda_{\max} t) \| = \lambda_{\max} t$ where $\lambda_{\max}$ is the leading eigenvalue of A. As G increases, the amplification at early times also increases thereby shifting the transition to the solution $\lambda_{\max} t$. The fact that disturbance amplification at early times never exceeds the asymptotic value as $t \to \infty$ suggests that the disturbance operator is only slightly non-normal. It is concluded from this example that the mechanism for instability proposed, which is directly related to a step increase in shear stress, is fundamentally a linear mechanism.

Unfortunately, the lack of quantitative experimental data on Marangoni driven fingering patterns precludes direct comparison to these predictions of the most unstable wavelength and the onset times for instability. Assuming that significant disturbance growth sets in at about a (dimensionless) time of $t \approx 30$, and extracting values from experiments for h_c^*, Π^*, μ^*, and L_c^* (Troian *et al.* 1989; Frank & Garoff 1995; He & Ketterson 1995; Fischer *et al.* 2001; Cachile *et al.* 2002) allows prediction of onset times for fingering which range roughly from 0.03 - 300 s. These predicted time scales for onset of instability are much more in line with experimental observations than all previous estimates based on sustained release according to $t^{1/2}$ (Fischer & Troian 2003*b*).

6. Conclusion

The analysis presented in this paper is designed to explore the fundamental cause of a dendritic fingering instability so commonly observed in thin viscous films driven to spread by a non-uniform distribution of surface active material at the gas-liquid interface. Experiments show that the spanwise instability nucleates and grows near the minimum in film thickness. Numerical studies indicate that this region is also characterized by an evolving spike in shear stress. Prior studies that have focused on a small and finite total mass of surfactant indicate that film spreading is asymptotically stable except possibly when van der Waals interactions are included. Recent studies suggest, however, that the instability triggered by van der Waals interactions is better described as a rupture instability and therefore very different than those observed in Marangoni driven systems. A more recent transient growth analysis based on sustained surfactant release according to $t^{1/2}$ has identified asymptotically unstable modes localized to the relevant thinned region but the onset times appear to be several orders of magnitude larger than experimental observations.

The current work examines the consequences of an infinite supply of surfactant to the spreading film by assuming a concentration distribution whose value at the origin is held fixed in time. The non-uniform spatial and temporal behavior of the evolving base states causes the generalized disturbance operator to be non-normal and non-autonomous. Both an approximate stability analysis which reduces the non-autonomous operator to autonomous form, as well as the complete time dependent analysis, clearly show positive perturbative growth of spanwise disturbances which localize to the region of large variation in shear stress. These disturbances undergo sustained amplification and asymptotic instability.

In order to identify the fundamental cause of instability, a simplified linear stability analysis is introduced which focuses exclusively on the behavior of a uniform thin film subject to a prescribed step change in shear stress. This model is shown to support traveling wave solutions which for a step increase (decrease) in shear stress are asymptotically unstable (stable). While only a select group of stress distribution functions are exam-

ined, it seems likely from these studies that the possibility of linearly unstable modes in thin films subject to a step increase in shear stress may signal a new type of interfacial instability.

The authors wish to thank the National Science Foundation (CTS and DMR), the NASA Microgravity Fluid Physics program and the US Army TACOM-ARDEC for financial support of this project. SMT also gratefully acknowledges the financial support and generous hospitality of the Moore Distinguished Scholar Program at the California Institute of Technology where this work was completed.

REFERENCES

Bertozzi, A. L. & Brenner, M. P. 1997 Linear stability and transient growth in driven contact lines. *Phys. Fluids* **9**, 530.

Borgas, M. S. & Grotberg, J. B. 1988 Monolayer flow on a thin film. *J. Fluid Mech.* **193**, 151.

Bull, J. L. & Grotberg, J. B. 2003 Surfactant spreading on thin viscous films: film thickness evolution and periodic wall stretch. *Expts. Fluids* **34**, 1.

Cachile, M., Schneemilch, M., Hamraoui, A. & Cazabat, A. M. 2002 Films driven by surface tension gradients. *Adv. Colloid Interface Sci.* **96**, 59.

Davis, J. M., Fischer, B. J. & Troian, S. M. 2003 General approach to the linear stability of thin spreading films. In *Interfacial fluid dynamics and transport properties* (ed. R. Narayanan & D. Schwabe), p. 79. Springer-Verlag, Berlin.

Davis, J. M. & Troian, S. M. 2003 On a generalized approach to the linear stability of spatially nonuniform thin film flows. *Phys. Fluids* **15**, 1344.

Dussaud, A. D., Matar, O. K. & Troian, S. M. 2005 Interfacial profile and spreading rate of a surfactant film advancing on a thin liquid layer: Comparison between theory and experiment. Submitted to JFM.

Espinosa, F. F. 1991 Spreading of surfactant in a pulmonary airway. *Advances in Bioengineering ASME* **20**, 571.

Farrell, B. F. & Ioannou, P. J. 1996*a* Generalized stability theory. Part I: Automnomous operators. *J. Atmos. Sci.* **53**, 2025.

Farrell, B. F. & Ioannou, P. J. 1996*b* Generalized stability theory. Part II: Nonautonomous operators. *J. Atmos. Sci.* **53**, 2041.

Fischer, B. J. 2003 Non-modal linear stability analysis of thin film spreading by marangoni stresses. PhD thesis, Princeton University.

Fischer, B. J., Darhuber, A. A. & Troian, S. M. 2001 Streamlets and branching dynamics in surfactant driven flow. *Phys. Fluids* **13**, S11.

Fischer, B. J. & Troian, S. M. 2003*a* Growth and decay of localized disturbances on a surfactant-coated spreading film. *Phys. Rev. E* **67**, 016309.

Fischer, B. J. & Troian, S. M. 2003*b* Thinning and disturbance growth in liquid films mobilized by continuous surfactant delivery. *Phys. Fluids* **15**, 3837.

Frank, B. & Garoff, S. 1995 Origins of complex motion of advancing surfactant solutions. *Langmuir* **11**, 87.

Fraysse, N. & Homsy, G. M. 1994 An experimental study of rivulet instabilities in centrifugal spin coating of viscous newtonian and non-newtonian fluids. *Phys. Fluids* **6**, 1491.

Gaver, D. P. & Grotberg, J. B. 1992 Droplet spreading on a thin viscous film. *J. Fluid Mech.* **235**, 399.

He, S. & Ketterson, J. 1995 Surfactant driven spreading of a liquid on a vertical surface. *Phys. Fluids* **7**, 2640.

Hindmarsh, A. C. 1983 Odepack, a systemized collection of ode solvers. In *Scientific Computing* (ed. R. S. Stepleman), p. 55. Amsterdam: North-Holland.

Huppert, H. E. 1982 Flow and instability of a viscous current down a slope. *Nature* **300**, 427.

Jensen, O. E. 1994 Self-similar, surfactant-driven flows. *Phys. Fluids* **6**, 1084.

Jensen, O. E. & Grotberg, J. B. 1992 Insoluble surfactant spreading on a thin viscous film : Shock evolution and rupture. *J. Fluid Mech.* **240**, 259.

Kalliadasis, S. & Homsy, G. M. 2001 Stability of free-surface thin-film flows over topography. *J. Fluid Mech.* **448**, 387.

Kataoka, D. E. & Troian, S. M. 1997 A theoretical study of instabilities at the advancing front of thermally driven coating films. *J. Coll. Int. Sci.* **192**, 350.

Kataoka, D. E. & Troian, S. M. 1998 Stabilizing the advancing front of thermally driven climbing films. *J. Coll. Int. Sci.* **203**, 335.

Matar, O. K. & Troian, S. M. 1997 Linear stability analysis of an insoluble surfactant monolayer spreading on a thin liquid film. *Phys. Fluids* **9**, 3645.

Matar, O. K. & Troian, S. M. 1998 Growth of non-modal transient structures during the spreading of surfactant coated films. *Phys. Fluids* **10** (4), 1234.

Matar, O. K. & Troian, S. M. 1999*a* The development of transient fingering patterns during the spreading of surfactant coated films. *Phys. Fluids* **11**, 3232.

Matar, O. K. & Troian, S. M. 1999*b* Spreading of a surfactant monolayer on a thin liquid film: Onset and evolution of digitated structures. *Chaos* **9** (1), 141.

Melo, F., Joanny, J. & Fauve, S. 1989 Fingering instability of spinning drops. *Phys. Rev. Lett.* **63**, 1958.

Pereira, A. M. 1995 An experimental investigation of a marangoni driven fingering instability in aqueous surfactant systems. Princeton University, b.S.E. thesis.

Schiesser, W. E. 1991 *The Numerical Method of Lines*. San Diego: Academic Press.

Shen, S. F. 1961 Some considerations of the laminar stability of incompressible time-dependent basic flows. *J. Aerospace Sci.* **28**, 397.

Troian, S. M., Herbolzheimer, E. & Safran, S. A. 1990 Model for the fingering instability of spreading surfactant drops. *Phys. Rev. Lett.* **65**, 333.

Troian, S. M., Wu, X. L. & Safran, S. A. 1989 Fingering instability in thin wetting films. *Phys. Rev. Lett.* **62**, 1496.

Warner, M. R. E., Craster, R. V. & Matar, O. K. 2002*a* Dewetting of ultrathin surfactant covered films. *Phys. Fluids* **14**, 1642.

Warner, M. R. E., Craster, R. V. & Matar, O. K. 2002*b* Unstable van der waals driven line rupture in marangoni driven thin viscous films. *Phys. Fluids* **14**, 4040.

Ye, Y. & Chang, H. C. 1999 A spectral theory for fingering on a prewetted plane. *Phys. Fluids* **11**, 2494.

TABLE 1. Results of the modal analysis for the most unstable wavenumber $Q_{\max}$ and growth rate $\beta(Q_{\max})$ within the reduced model for representative values of the upstream shear stress G, $h_\infty = 1/6$ and $\delta = 0.1$, as defined in the text.

G	$Q_{\max}$	$\beta_{\max}$
0.5	0.20	0.007
1.0	0.35	0.037
2.0	0.50	0.130

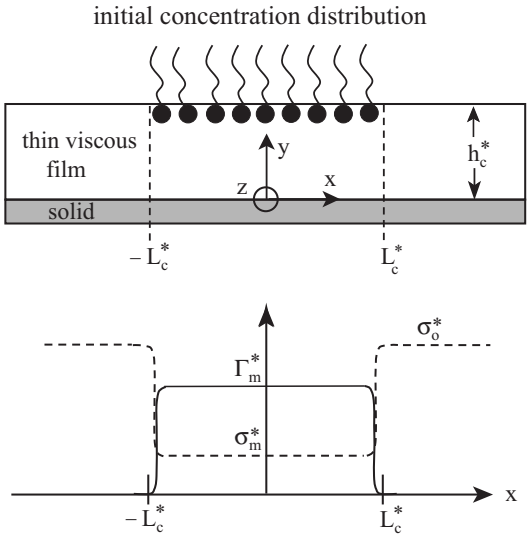

FIGURE 1. Schematic diagram of the initial configuration for film spreading in rectilinear geometry. A viscous film of initial thickness h_c^*, viscosity μ^* and density ρ^* is partially coated from $-L_c^* \leqslant x \leqslant L_c^*$ by an insoluble surfactant monolayer. The initial concentration distribution is given by Γ_m^*, which decays to zero beyond $\pm L_c^*$. The surface tension of the coated film is reduced from σ_o^* to σ_m^*. The maximum spreading pressure responsible for film mobilization is given by $\Pi^* = \sigma_o^* - \sigma_m^*$. In this study, the surfactant concentration at the origin is held fixed at the value Γ_m^* to simulate an infinite supply of surfactant to the spreading film.

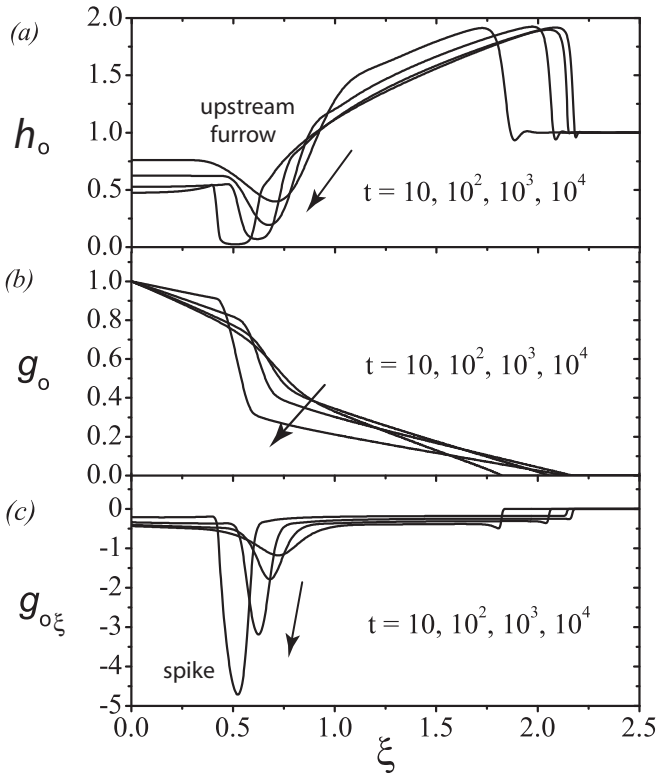

FIGURE 2. Numerical solutions of the non-dimensional base states for *(a)* film thickness h_o, *(b)* surfactant concentration g_o and *(c)* concentration gradient $g_{o\xi}$ (also equivalent to the negative value of the shear stress) for times ranging from 10 to 10^4. Additional parameter values are $a = 0.45$, $b = 0$, $Pe_s = 1000$ and $\mathcal{C} = 10^{-4}$.

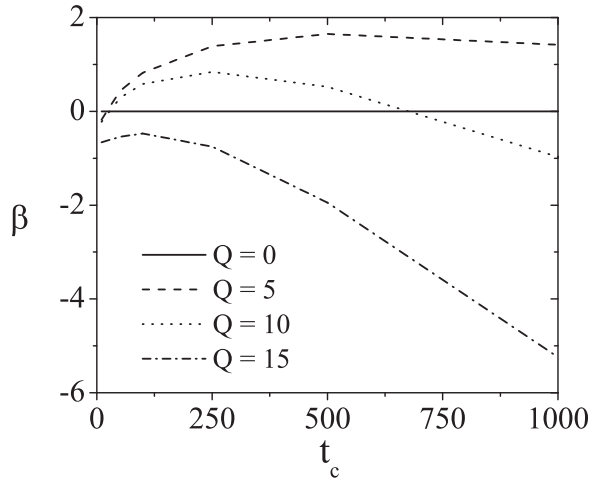

FIGURE 3. Numerical solution of the instantaneous growth rate, $\beta(Q, t_c)$ for $0 \leqslant Q \leqslant 15$. The times, t_c, represent the fixed time at which the eigenfunctions and eigenvalues of the linearized disturbance operator are evaluated.

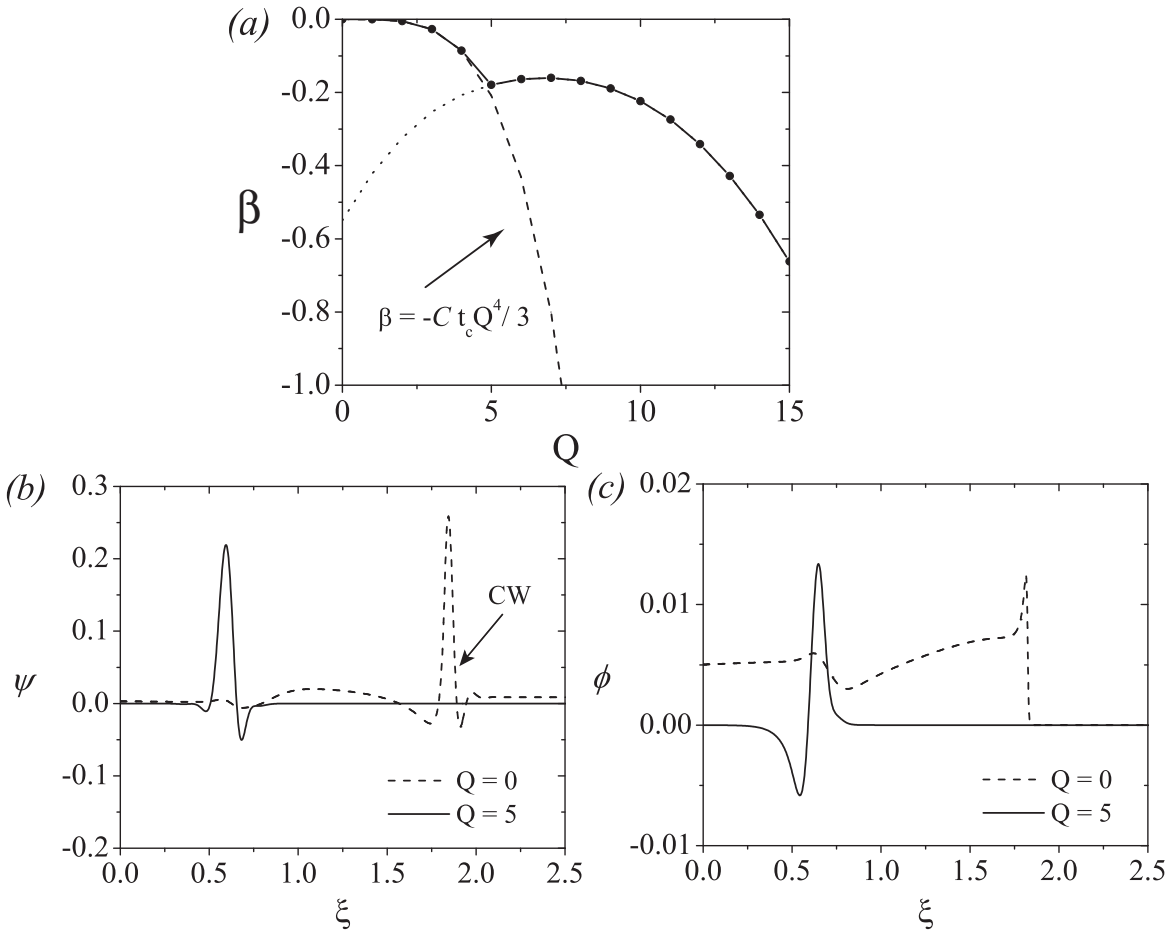

FIGURE 4. Numerical solutions of disturbance *(a)* growth rate $\beta(Q)$, *(b)* film thickness $\psi(\xi)$, and *(c)* concentration profile $\phi(\xi)$ for $t_c = 10$. The dashed line in *(a)* represents the continuous mode [capillary-like wave (CW)] solution given by (3.5) and the dotted line denotes solutions corresponding to the discrete spectrum. Other parameter values are $Pe_s = 1000$ and $\mathcal{C} = 10^{-4}$.

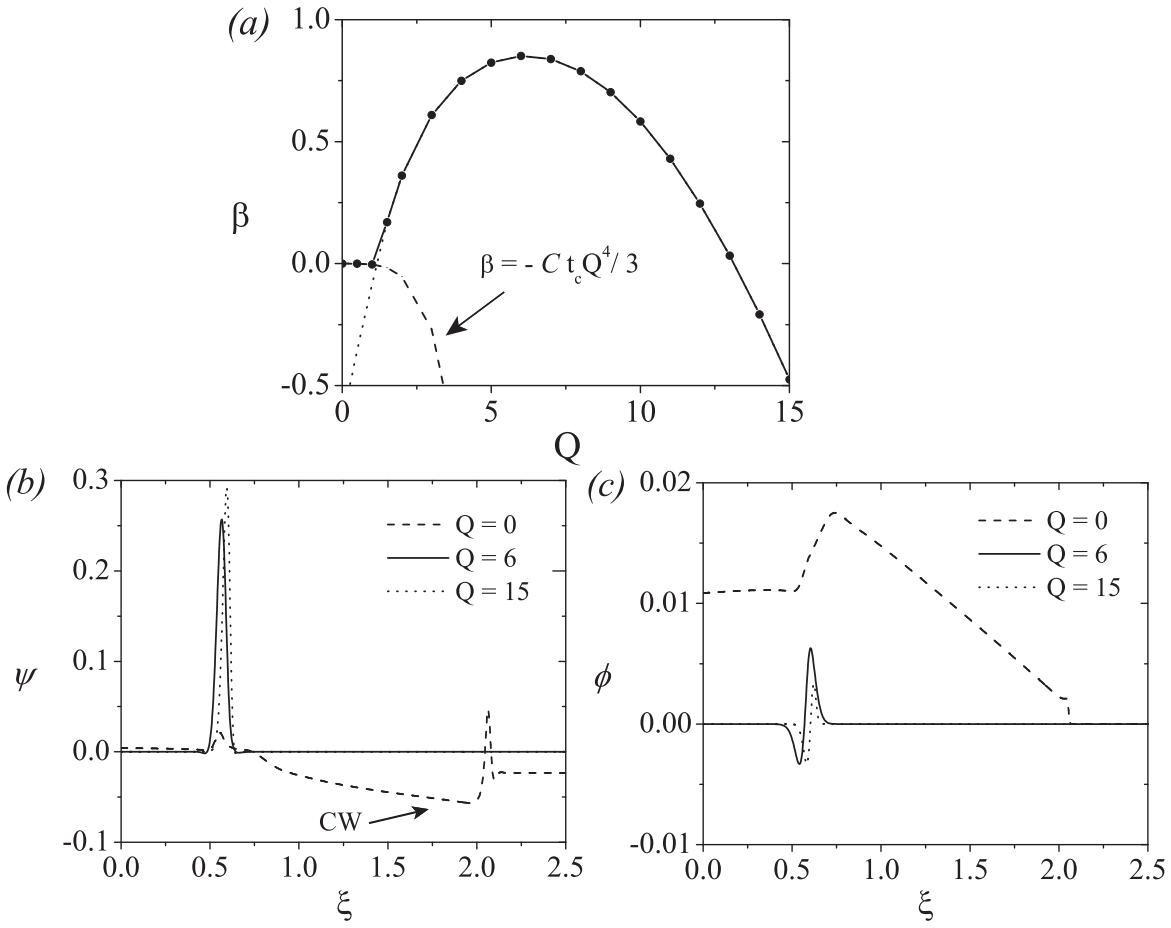

FIGURE 5. Numerical solutions of disturbance *(a)* growth rate $\beta(Q)$, *(b)* film thickness $\psi(\xi)$, and *(c)* concentration profile $\phi(\xi)$ for $t_c = 100$. The dashed line in *(a)* represents the continuous mode [capillary-like wave (CW)] solution given by (3.5) and the dotted line denotes solutions corresponding to the discrete spectrum. Other parameter values are $Pe_s = 1000$ and $\mathcal{C} = 10^{-4}$.

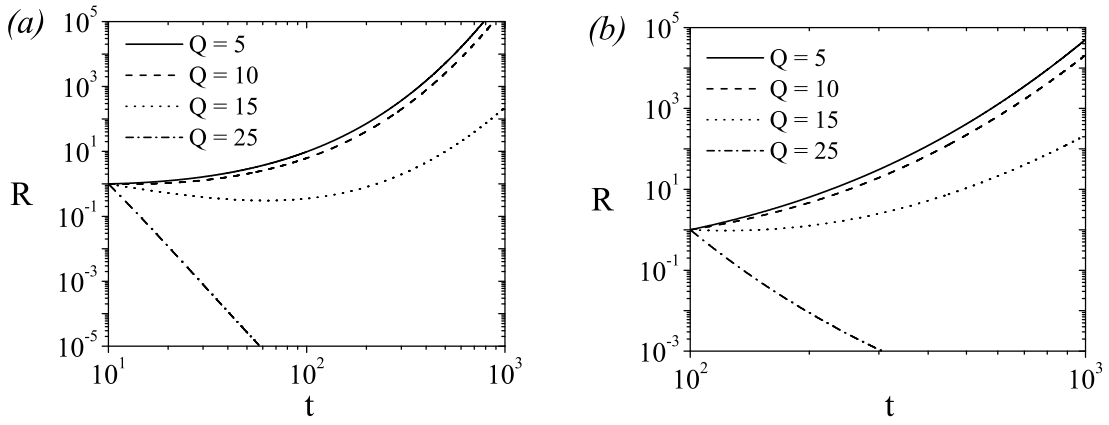

FIGURE 6. Numerical solutions of the normalized disturbance amplification ratio for $5 \leqslant Q \leqslant 25$. The perturbations are prescribed at times *(a)* $t_i = 10$ and *(b)* $t_i = 100$. Other parameter values are $Pe_s = 1000$ and $\mathcal{C} = 10^{-4}$.

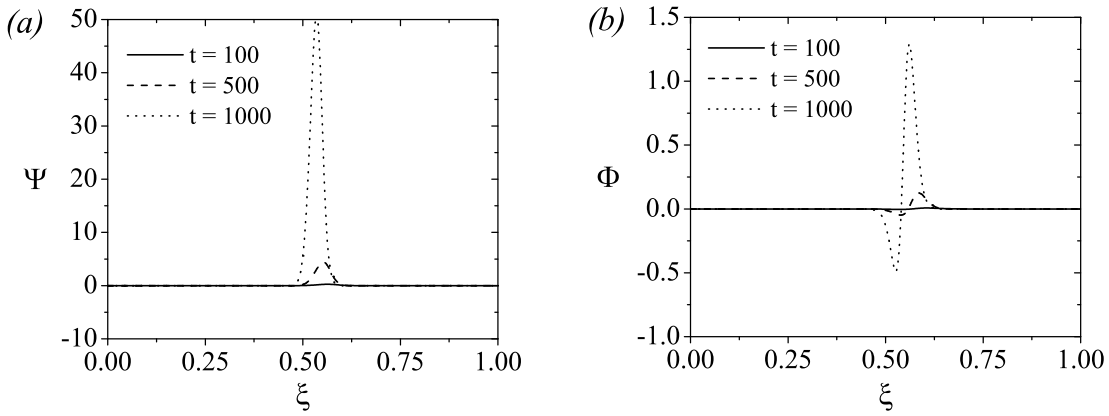

FIGURE 7. Plots of the evolution of *(a)* disturbance film thickness Ψ and *(b)* disturbance surface concentration Φ for $Q = 1$ and $t_i = 100$. Other parameter values are $Pe_s = 1000$ and $\mathcal{C} = 10^{-4}$.

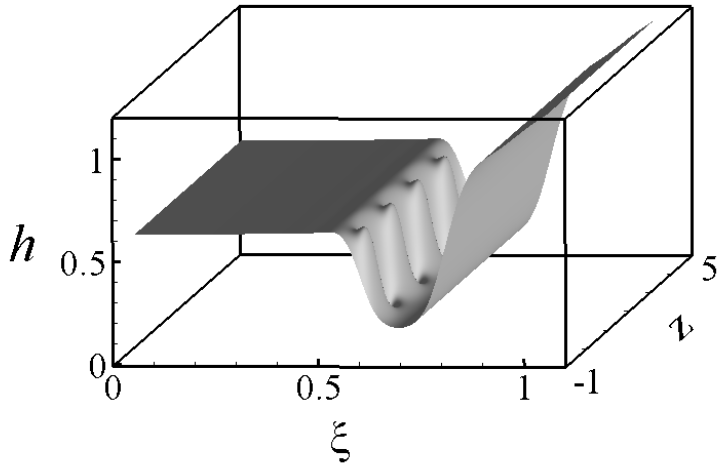

FIGURE 8. Film thickness profile $h(\xi, z, t)$ including disturbance at $t = 500$ for $Q = 5$ and $\tilde{\delta} = 0.01$. Significant corrugations appear just upstream of the minimum in film thickness. Other parameter values are $Pe_s = 1000$ and $\mathcal{C} = 10^{-4}$.

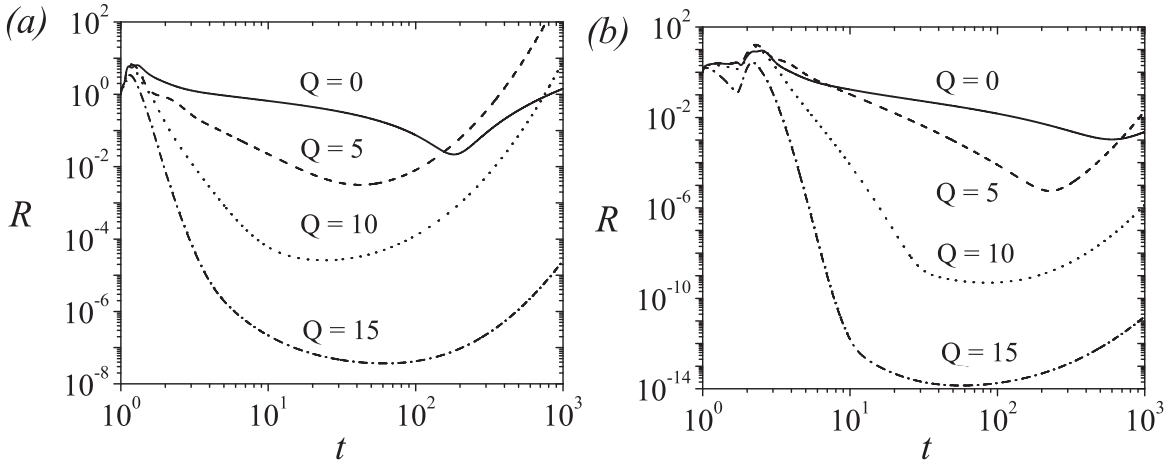

FIGURE 9. Evolution of disturbance amplification R for gaussian perturbations initially situated at *(a)* $\xi_s = 1.0$ and *(b)* $\xi_s = 2.0$ as a function increasing wavenumber Q.

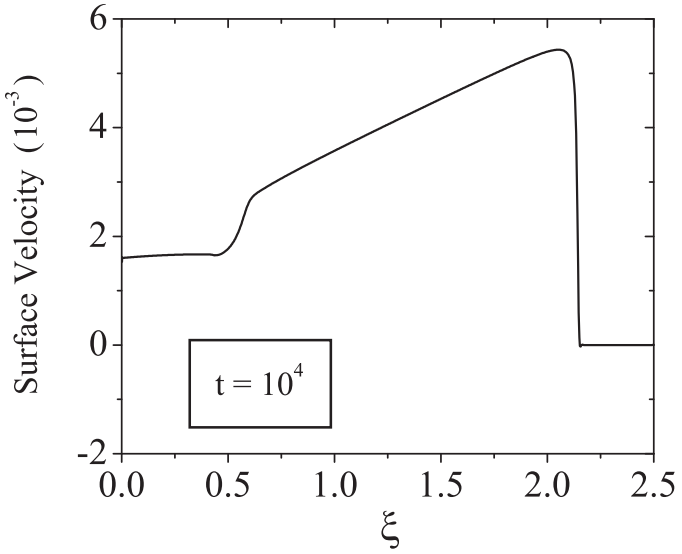

FIGURE 10. Base-state surface flow speed at $t = 10^4$ for the concentration profile and boundary conditions specified in the text. Other parameter values are $Pe_s = 1000$ and $\mathcal{C} = 10^{-4}$. There is evident a step increase in speed near the region of maximum film thinning and a step down in film speed at the leading edge of the surfactant monolayer which joins the undisturbed film.

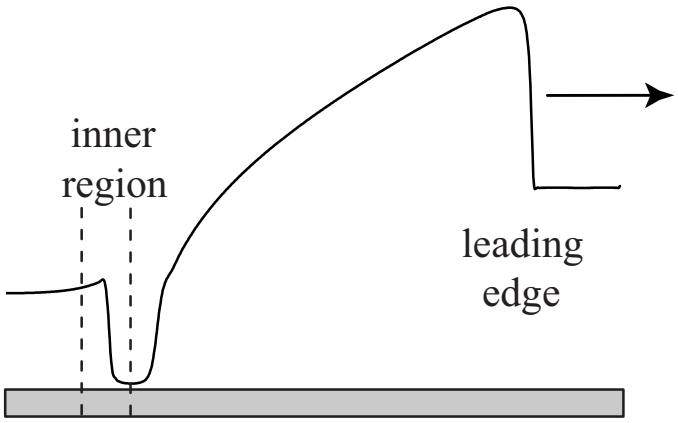

FIGURE 11. Schematic diagram showing two important regimes in the evolving film thickness profile. These include an inner region situated near the pinch point where the film demonstrates a sharp drop in film thickness and a bulge at the leading edge which signals the transition between the (surfactant) coated and un-coated portions of the film.

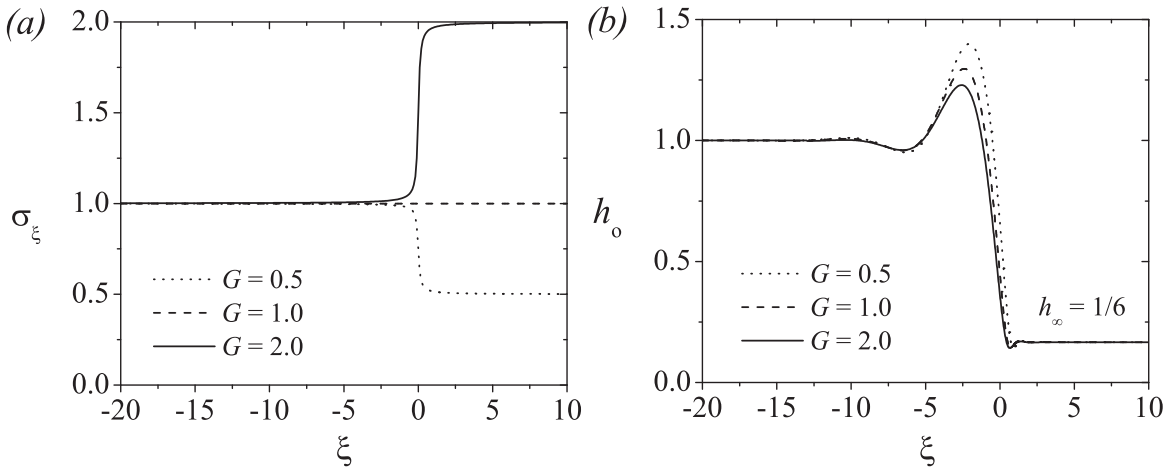

FIGURE 12. *(a)* Prescribed shear stress distribution σ_ξ which demonstrates a step change in value near $\xi = 0$. *(b)* Solution of the base-state film thickness $h_o(\xi)$ for $h_\infty = 1/6$, $\delta = 0.1$ and $G = 0.5, 1.0$ and 2.0 within the reduced model.

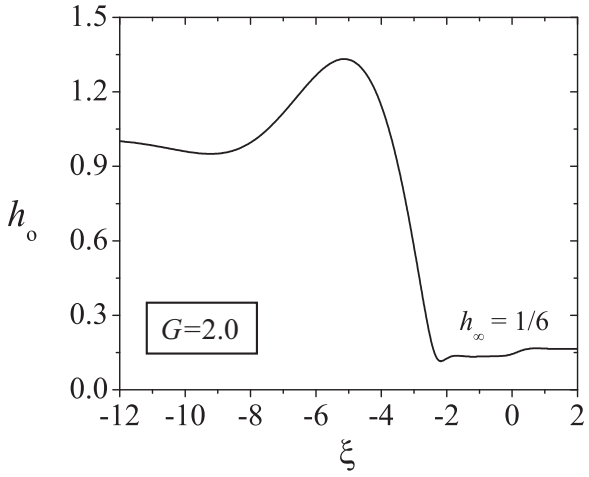

FIGURE 13. A second base-state solution $h_o(\xi)$ for $h_\infty = 1/6$, $\delta = 0.1$ and $G = 2.0$ within the reduced model.

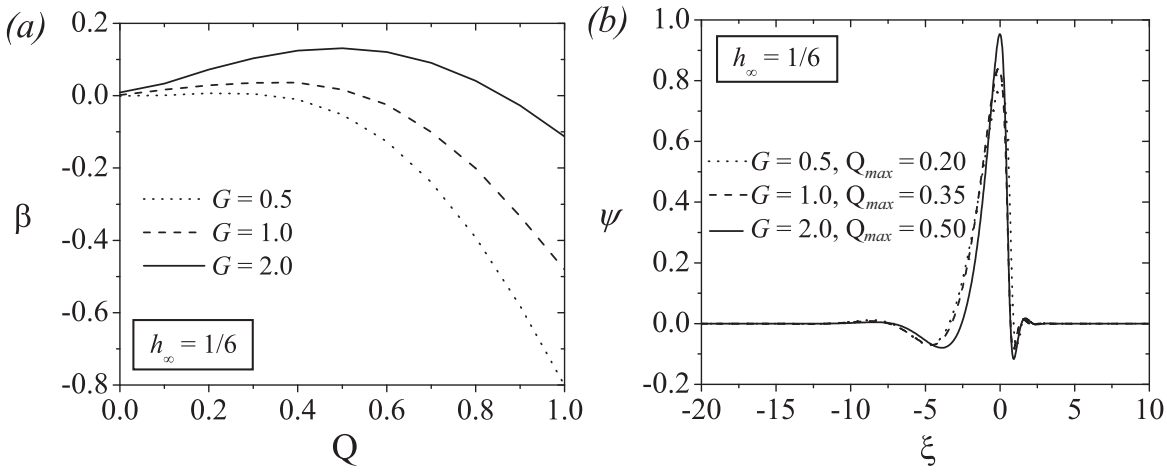

FIGURE 14. Solutions for the reduced model corresponding to *(a)* the eigenvalues $\beta(Q)$ and *(b)* eigenfunctions with maximum growth rate $\psi(Q_{\max})$ for $h_\infty = 1/6$, $\delta = 0.1$ and $G = 0.5, 1.0$ and 2.0.

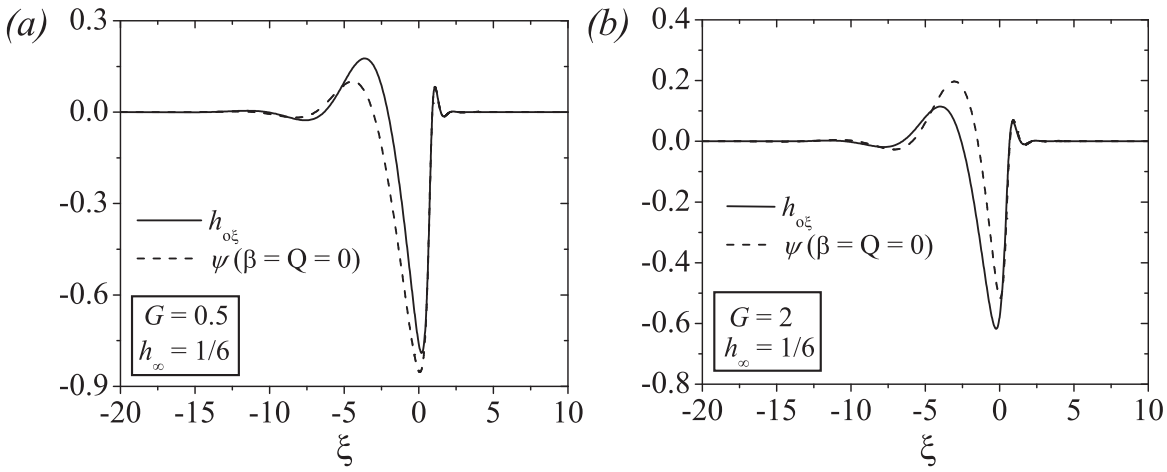

FIGURE 15. Comparison between the shapes of the neutrally stable mode and $h_{o\xi}$ for *(a)* $G = 0.5$ and *(b)* $G = 2.0$ with $h_\infty = 1/6$ and $\delta = 0.1$.

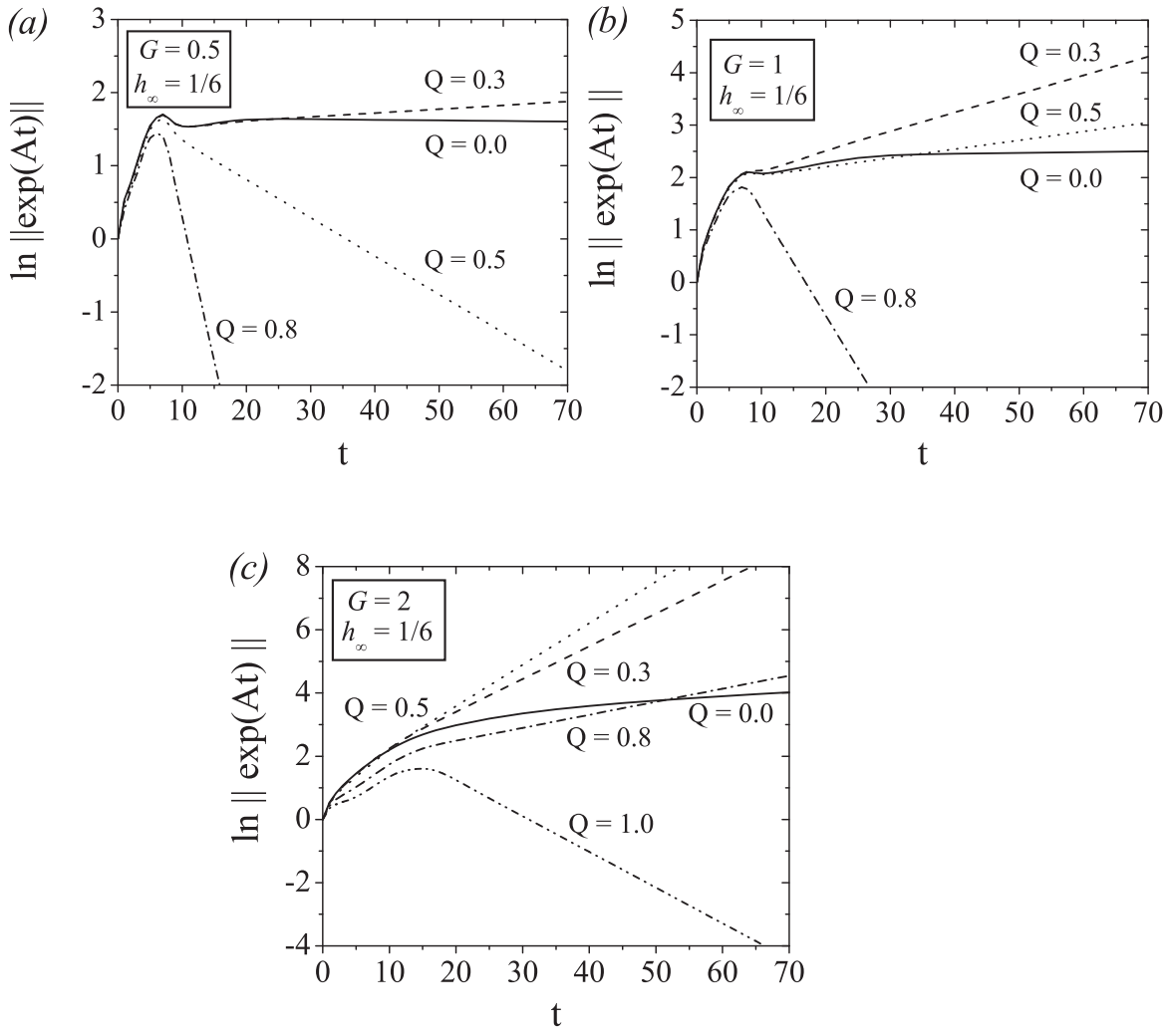

FIGURE 16. Evolution of amplification curves corresponding to optimal disturbances wavenumber perturbations for *(a)* $G = 0.5$, *(b)* $G = 1.0$, and *(c)* $G = 2.0$ as a function of increasing wavenumber Q for $h_\infty = 1/6$ and $\delta = 0.1$.